Egyptian Journal of Chemistry

http://ejchem.journals.ekb.eg/

The Detection of NH_3, H_2S and HBr Gases by Carboxymethyl Cellulose Sodium / ZnO Nanocomposites: A Theoretical Study

Rania Badry[1]*, Nadra Nada[1], Mahmoud M. El-Nahass[2], Hanan Elhaes[1] and Medhat A. Ibrahim[2, 4]

[1]*Physics Department, Faculty of Women for Arts, Science and Education, Ain Shams University, 11757 Cairo, Egypt.*

[2]*Physics Department, Faculty of Education, Ain Shams University, Roxy, Cairo, Egypt*

[3]*Nanotechnology Research Centre (NTRC), The British University in Egypt (BUE), Suez Desert Road, El-Sherouk City, Cairo, 11837, Egypt.*

[4]*Molecular Spectroscopy and Modeling Unit, Spectroscopy Department, National Research Centre, 33 El-Behouth St., 12622, Dokki, Giza, Egypt*

Abstract

Toxic gases, such as ammonia (NH_3), hydrogen sulphide (H_2S) and hydrogen bromide (HBr) gases, even at very low gas concentrations, have harmful effects on human health. Accordingly, environmental monitoring, industrial plants, automotive, air quality assurance technology, and various low-concentration gases must be reliably detected. The effect of NH_3, H_2S and HBr gases on the sensitivity of carboxymethyl cellulose sodium (CMC) nanocomposites has been studied theoretically using density functional theory (DFT) at B3LYP/Lanl2dz basis set. Total dipole moment (TDM), electronic band gap energy (ΔE) and molecular electrostatic potentials (MESPs) for CMC, CMC/ZnO and CMC/ZnO/ different gases are calculated. The results showed that the sensitivity of CMC increased due to the interaction with ZnO molecules through both complex and adsorb interactions, as TDM of CMC increased to35.1708 Debye and ΔE decreased to0.2645 eV. Also, TDM increased to 28.7687, 31.5937 and 32.8856 Debye upon the exposure of the CMC/ ZnO surface to NH_3, H_2S and HBr gases respectively. Additionally, MESP maps confirmed the results of the electronic properties where the sensitivity increased due to the increment in the dimer CMC electronegativity. Therefore, the proposed CMC/ ZnO structure could be used as a sensor for NH_3, H_2S and HBr gases.

Keywords: NH_3; H_2S; HBr; CMC/ZnO; DFT; TDM and Band gap energy.

1. Introduction

In recent years, a lot of research has been conducted on exploring new materials with high sensitivity to detect toxic gases. Nanomaterials have novel mechanical, electrical, and optical properties compared to their bulk counterpart [1-3]. These novel characteristics of nanomaterials are believed to be due to the quantum confinement effect and the higher surface area to volume ratio [4,5]. Transition metals oxides are an important branch of semiconductors because they have applications in many fields, such as energy storage devices, solar cells, capacitors, sensors, electrochemical devices, electronics, and catalysis [6-9]. Among the transition metal oxides, zinc oxide nanoparticles are of widespread interest because of their unique chemical and physical characteristics, bringing about opportunities for environmental, energy, and electrical applications such as sensors and solar cells [8,9], biomedical, and wastewater treatment applications [10-12].

ZnO importance comes from its high conductance, good thermal and mechanical stability, large exciton binding energy of 60 MeV and a wide direct band gap of 3.37 eV [13-15]. ZnO has good resistance to radiation and is environmentally friendly

*Corresponding author e-mail: raniabadry806@gmail.com.; (Rania Badry).

Receive Date: 31 October 2021, Revise Date: 05 March 2022, Accept Date: 07 December 2021, First Publish Date: 07 December 2021

DOI: 10.21608/EJCHEM.2021.103668.4797

[16,17]. Additionally, it is widely applied in cosmetics, pharmaceutics, food science, optoelectronics, agriculture fields [18-20] and transparent UV protection films [21]. Among these applications, ZnO nanostructures can be used to detect hydrogen sulphide(H_2S) gas in the air [22]. Research has suggested that nanocomposites based on polymer/ metal oxides enhance the polymer's properties so far.

Most of polysaccharides have been studied in membrane preparation as a polymer host [23]. Polysaccharide membranes have potential applications in solar cells, electric double layer capacitors, sensors, and solid-state batteries [24]. One of the most interesting polysaccharides is carboxymethyl cellulose sodium (CMC). CMC is a natural polysaccharide polymer and usually recognized as cellulose gum. Also, it is one of cellulose derivatives and is derived from cellulose through alkalization process followed by carboxymethylation processes [25,26]. Since CMC has very important characteristics, including being non-toxic, biodegradable, inexpensive, tasteless, odourless,water soluble, highly viscos,highly transparent, and has high degree of amorphousity, it is, therefore, considered a very important polymer for everyday life. It has a very wide range of industrial applications, including pharmaceutics, cosmetics, thickener and stabilizers for beverages and foods, textiles, paper, adhesives, and paints [25-27]. Because of these features, CMC is considered a promising material because of its properties which are advantageous for humanity [27-29].

In the past few decades, the latest advances in the detection of toxic gases have been categorized through highly explored detection materials and techniques. Molecular modeling (MM) is one of the most rapidly progressing areas in science. MM covers several fields among them computational chemistry, drug design, computational biology, nanostructures, and materials science [30-32]. MM can help to bring the primary experimental data and provide a complete physical picture and to make a connection between experimental and theoretical work [33,34]. Disadvantages of experimental work such as hazards of dealing with either explosive, or harmful substances and consuming both time as well as cost are overcome using computational modeling [35].

Over recent years, molecular modelling, in addition to the other experimental techniques, has been utilised to investigate biopolymers as well as synthetic polymers. Many research papers focused on optimizing models of cellulose and other polymers and studying their chemical, physical, electronic, and thermal properties [36].

IbrahimM.et al. (2011) constructed a theoretical model molecule for cellulose, chitosan, cellulose blended with chitosan, cellulose blended with ZnO (TiO_2), chitosan blended with ZnO (TiO_2) and cellulose/chitosan/ ZnO (TiO_2) to study the effect of polymerization degree. The results indicated that both TDM and the band gap energy are changed, and the reactivity is continuously increased due to the addition of ZnO (TiO_2) to the blended polymers [37].

Ibrahim M.A. et al. (2018) proposed a model for graphene and graphene decorated with several oxides of alkali metals including: CaO, MgO and SrO. The results indicated that there were enhancements in the calculated physical quantities which confirmed the suitability of the supposed structure of graphene for application as a gas sensor for H_2S [38]. Finally, this article aims to study theoretically the possibility of using CMC/ ZnO nanocomposite as a sensor for ammonia (NH_3), H_2S and hydrogen bromide (HBr) gases.

Calculation details.

The improvement in the electronic properties of CMC is achieved by the addition of a ZnO molecule due to its novel properties. Accordingly, for accurate predictions, this study is carried out with Density Functional Theory methods (DFT) at B3LYP level of theory [39-41] with Lanl2dz basis set [42,43]. The CMC, CMC/ZnO, CMC/ZnO/NH_3, CMC/ZnO/H_2S and CMC/ZnO/HBr models are subjected to optimization using Gaussian 09 software [44]. Total dipole moment (TDM), electronic band gap energy (ΔE) and molecular electrostatic potentials (MESPs) are calculated for all proposed structures at Molecular Modeling and Spectroscopy Unit, Spectroscopy Department, National Research Centre, Cairo, Egypt.

Results and discussion

1.1. Building model molecules

The first goal in this study is to understand the mechanism of surface interaction between CMC and ZnO. Based on the previous studies, it is concluded that the interaction between polymers and different metal oxides is processed throughout the oxygen atom of the metal oxide [45-49]. Accordingly, two units of CMC (dimer CMC) and one ZnO molecule are supposed to interact with each other as complex and adsorb state.

1.2. Calculated physical parameters

Figure 1-a, 1-b and 1-c presents the structure,distribution of the electrons in HOMO/LUMO and MESP maps respectively for dimer CMC. As presented in table 1 dimer CMC has TDM of 9.0737 Debye and ΔE of 0.4493 eV. To

study the reactivity of the molecule it is necessary to define the active sites within the studied molecule and, subsequently, the interaction with other molecules will be clear and easy to be understood.

The molecule's reactivity is best described by the MESP maps. Where the MESP maps are described by colour range starting from red to blue, such that the red colour represents the electron rich regions (high negative MESP), the blue ones describe the proton rich regions (low negative MESP) [50-52]. Therefore, based on the obtained MESP maps of dimer CMC, eight active sites are found in the proposed dimer CMC structure. These active sites are the hydroxyl groups (-OH-) located at carbon atoms number 4 (i.e.P1), 5 (i.e. P2), 58 (i.e. P3), 67 (i.e. P4) and 68 (i.e.P5), C=O group (i.e., P6 and P7) and finally the -O- linkage along the chain (i.e. P8).

As presented in figure 1-c the red colour density is very high around the oxygen atoms mentioned above than the others. This is due to the electro-negativity of oxygen atoms and vice versa for the hydrogen atoms that have a highly positive nature. Accordingly, ZnO molecules can interact with dimer CMC through these positions. Figure 2-a, 2-b and 2-c presents the structure,**HOMO/LUMO molecular orbitals** and MESP respectively of dimer CMC / (P1)complexed OZn.This structure has TDM, and ΔE of 31.5836Debye and 0.2637eV respectively, as presented in table 1. However, in the case of the adsorption mechanism, TDM becomes 28.3728Debye, and ΔE equals 0.2444eV as tabulated in table 2.The structure representing dimer CMC / (P1)adsorbed OZn is illustrated in figure 2-d while figure 2-e and 2-f presents its ΔE and MESP maps.The MESP of dimer CMC /P1 OZn in the two mechanisms shows that the dimer CMC structure possesses a dense red coloursurrounding the whole model upon the interaction with OZn, and that the intensity of the colour increased around the OH group attached to carbon atom number 4. According to thestated results, the sensitivity of dimer CMC/ P1 OZn model molecule, in both complex and adsorb interaction, increased strongly and the structure became more reactive than that of dimer CMC.

Similarly, Figures 3-a and 4-a present the dimer CMC structure complexed with OZn through the OH group attached to C atoms number 5 and 58, respectively. While figures 3-d and 4-d present the dimer CMC structure interacting weakly with OZn. The distribution of electrons (HOMO/LUMO) within the molecular orbitalis is presented in figures 3-b and 4-b for dimer CMC/ P2 and P3complexed OZn, and in figures 3-e and 4-e for dimer CMC/ P2 and P3 adsorbed OZn respectively. Also, the values of TDM and ΔE are illustrated in table 1 for dimer CMC complexed with OZn table 2 contains the same electronic parameters for dimer CMC adsorbed with OZn in all possible active sites,where it is found that dimer CMC/ P2 OZn has TDM of 35.1708 and 30.9937 Debye and ΔE of 0.2645 and 0.2550 eV for complex and adsorb interactions respectively.

Meanwhile, TDM and ΔE of dimer CMC/ P3 OZn are11.2919Debye and 0.5127eV respectively for complex interaction and 8.0315 Debye and 0.4125 eV for weak interaction.The MESP for dimer CMC/ P2 OZn and dimer CMC/ P3 OZn are presented in figures 3-c and 4-c, respectively for complex interaction while figures 3-f and 4-f present the MESP maps for the adsorb structures of dimer CMC/ P2 OZn and dimer CMC/ P3 OZn. MESP maps indicated that the reactivity continuously changed with changing the interaction site and that the highest reactivity is that for dimer CMC/ P2 OZn. As the oxygen atom number 5 in dimer CMC/ P2 OZn model showed a dense red colour after the interaction with ZnO instead of the yellow colour (in both cases of interaction), that refers to its high electro-negativity. This confirms that after the interaction, the charges of both dimer CMC and ZnO undergo redistribution that confirms the TDM and energy gap results.

Table 1 TDM as (Debye) and HOMO/LUMO energy gap as (eV)calculated at B3LYP/LANL2DZ for Dimer CMC and Dimer CMC/ PY OZn throughout the complex interaction where, Y refers to the position of OH group through which the interaction proceed(Y=1:5), Y=6 and 7 refers to that proceeds through C=O group and Y= 8 to those proceeds through O linkage.

Structure	**TDM (Debye)**	**ΔE (eV)**
Dimer CMC	9.0737	0.4493
Dimer CMC/ P1OZn	31.5836	0.2637
Dimer CMC/ P2OZn	35.1708	0.2645
Dimer CMC/ P3OZn	11.2919	0.5127
Dimer CMC/ P4OZn	22.9653	0.2419
Dimer CMC/ P5OZn	22.7157	0.2781
Dimer CMC/ P6OZn	9.9434	0.4506
Dimer CMC/ P7OZn	14.2952	0.2427
Dimer CMC/ P8OZn	15.1924	0.5581

Table 2TDM as (Debye) and HOMO/LUMO energy gap as (eV)calculated at B3LYP/LANL2DZ for Dimer CMC and Dimer CMC/ PY OZn throughout theadsorb interaction where, Y refers to the position of OH group through which the interaction proceeds(Y=1:5), Y=6 and 7 refers to that proceeds through C=O group and Y= 8 to those proceeds through O linkage.

Structure	TDM (Debye)	ΔE (eV)
Dimer CMC/ P1OZn	28.3728	0.2444
Dimer CMC/ P2OZn	30.9937	0.2550
Dimer CMC/ P3OZn	8.0315	0.4125
Dimer CMC/ P4OZn	12.9167	0.2359
Dimer CMC/ P5OZn	20.7476	0.2378
Dimer CMC/ P6OZn	12.4820	0.3252
Dimer CMC/ P7OZn	17.1858	0.3883
Dimer CMC/ P8OZn	18.8514	0.4430

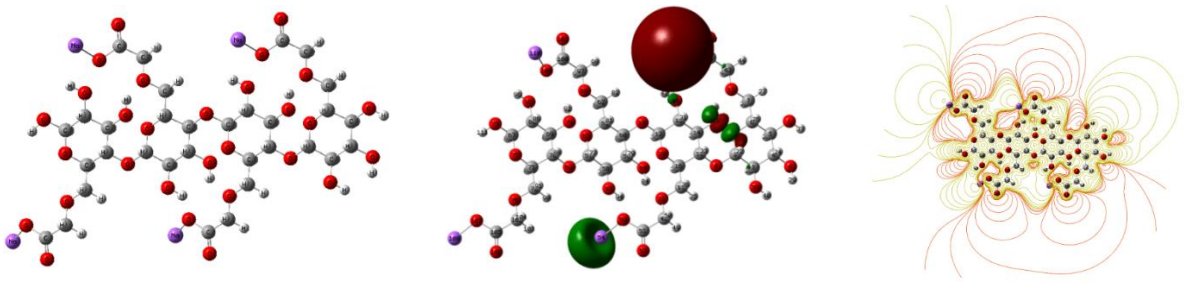

(a) (b) (c)

Fig. 1.a)- Optimized structure; b)- MESP; andc)- HOMO-LUMO orbitals of dimer CMCcalculated at B3LYP/Lanl2dz.

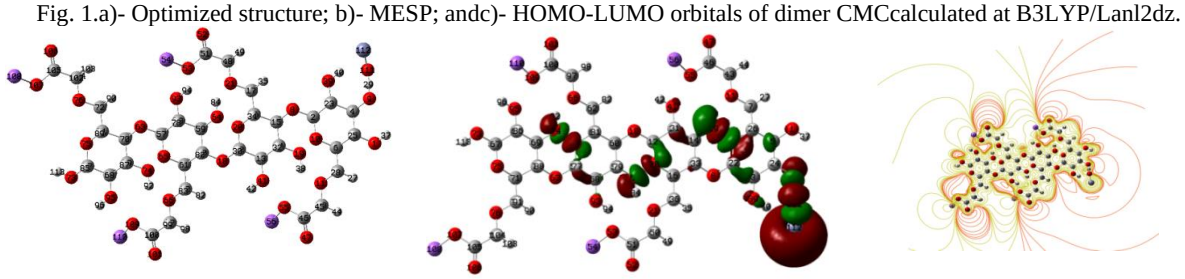

(a) (b) (c)

Complex state

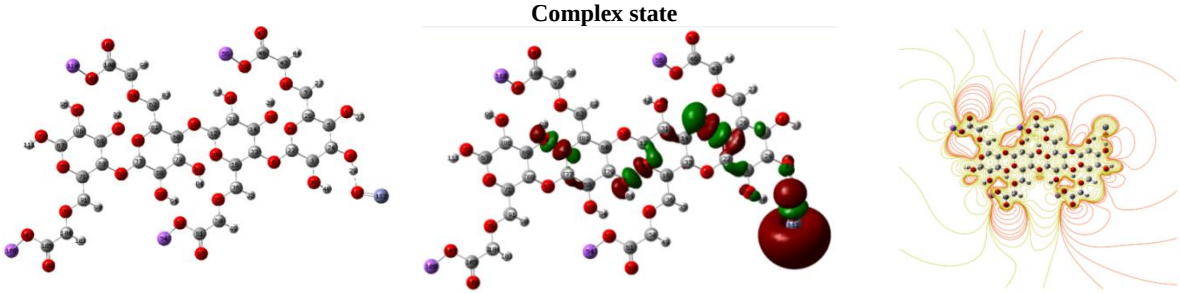

(d) (e) (f)

Adsorb state

Fig. 2. a) and d)- Optimized structure; b) and e)- HOMO-LUMO orbitals;and c) and f)- MESP maps calculated at B3LYP/LANL2DZ for dimer CMC/ P1 OZn in the two interaction mechanisms.

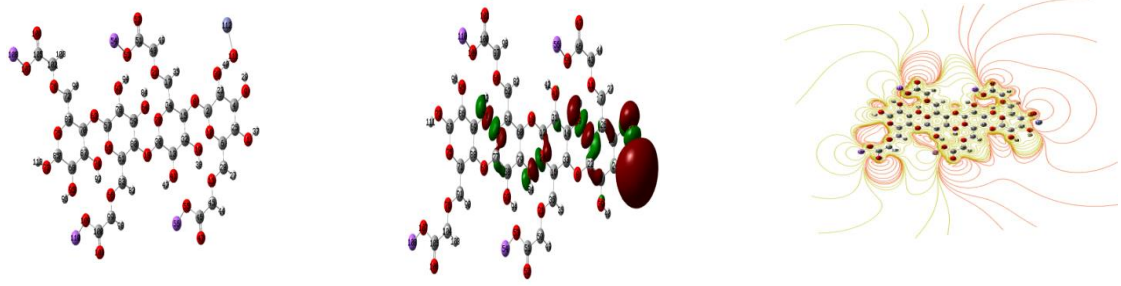

(a) (b) (c)

Complex state

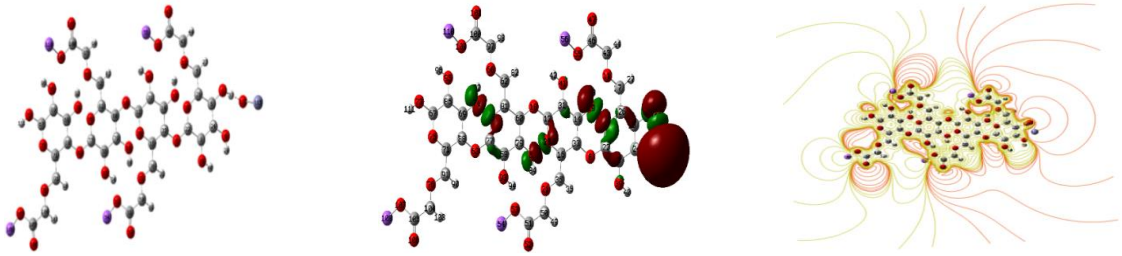

(d) (e) (f)

Adsorb state

Fig. 3.a) and d)- Optimized structure; b) and e)- HOMO-LUMO orbitals; and c) and f)- MESP maps calculated at B3LYP/LANL2DZ for dimer CMC/ P2 OZn in the two interaction mechanisms.

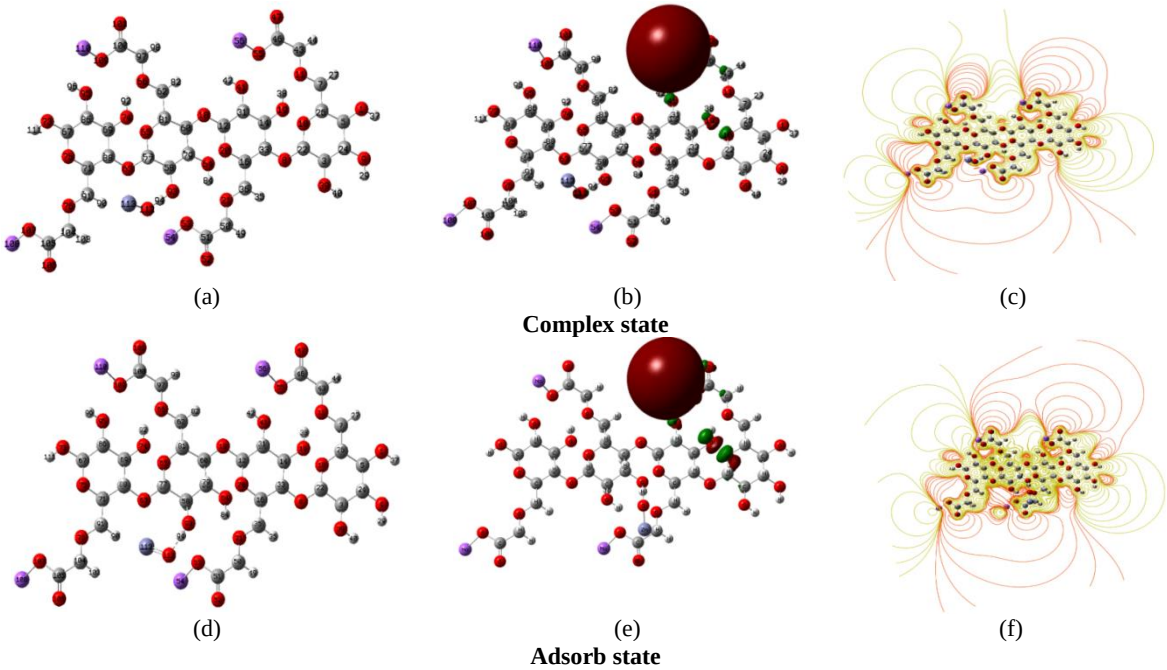

Fig. 4. a) and d)- Optimized structure; b) and e)- HOMO-LUMO energy; and c) and f)- MESP maps calculated at B3LYP/LANL2DZ for dimer CMC/ P3 OZn in the two interaction mechanisms.

The structures supposed to represent dimer CMC complexed with OZn via OH group number 67 and 68 are presented in figures 5-a and 6-a. The adsorbed structures of dimer CMC/ P4 OZn and dimer CMC/ P5 OZn are presented in figures 5-d and 6-d, respectively, where both have TDM of22.9653 and 22.7157Debye and ΔE of 0.2419 and 0.2781eV in case of complex interaction respectively. However, for the adsorption mechanism, dimer CMC/ P4 OZn has TDM of 12.9167 and ΔE of 0.2359 eV and dimer CMC/ P5 OZn has TDM of 20.7476 Debye and ΔE of 0.2378 eV. Also, the electrons distribution in the orbitals for both are presented in figures 5-b and 6-b respectively. Meanwhile, their MESP maps are presented in figures 5-c and 6-c and show that the reactivity increased slightly in comparison with that of dimer CMC, dimer CMC/ P1 OZn and dimer CMC/ P2 OZn, where the red colour intensity increased slightly around the oxygen atom connected to the OZn molecule and the terminals remained neutral.

On the other hand, for the interactions proceeding through the C=O group, the changes in TDM are very small in some sites. When the interaction proceeds through the C=O group located at C atom number 52 (dimer CMC/ P6 OZn),TDM calculated is 9.9434 and 12.4820 Debye but the changes in the ΔEare ineffective where they became 0.4506 and 0.3252 eV for complex and adsorb interactions respectively. Figure 7 and figure 8 show the structure, ΔE and MESP for the two probabilities of interaction that proceed through C=O groups located at C atom numbers 52 and 100 respectively (in both cases complex and adsorbed one). However, the C=O group present at C atom number 100 (dimer CMC/ P7 OZn) has TDM of 14.2952 Debye and ΔE of 0.2427 eV for complex interaction. Meanwhile, for the adsorbed interaction, TDM becomes 17.1858 Debye and ΔE is 0.3883 eV. Finally, for the interaction proceeding through the -O- linkage along the chain (dimer CMC/ P8 OZn),it has TDM of 15.1924 Debye and ΔE of 0.5581 eV for complex interaction and TDM of 18.8514 Debye and ΔE of 0.4430 eV for adsorbed one. Figure 9(a, b and c) shows the model molecule presenting the dimer CMC structure interacting with OZn (complex interaction) via the -O- group located along the chain, ΔE and MESP maps. For the adsorbed mechanism, Figure 9-d, e and f shows the structure, ΔE and MESP maps for dimer CMC/ P8 OZn.

Based on the results, it could be concluded that the sensitivity of dimer CMC is increased upon the interaction with ZnO nanoparticles,since TDM of dimer CMC increased approximately to triple its value due to the interaction with ZnO and vice versa for the ΔEas it decreased to half of its value. As presented in table 1 and table 2, it is found that both TDM and the ΔE changed according to the interaction sites. Additionally, from the calculated parameters, we can conclude that the interaction between CMC and ZnO is an adsorption interaction

rather than complex. As the adsorption model molecules have slightly small band gap values, in comparison with those of complex one, we can start to increase the number of ZnO molecule to 2 and 3 units starting from dimer CMC/ P2 OZn. Figure 10-a and b shows the models presenting dimer CMC/ 2 OZn and dimer CMC/ 3 OZn respectively. It is found that the TDM values decreased to 12.7279 and 13.6132 Debye for dimer CMC interacted with two and three units of ZnO molecules respectively, while ΔE decreased to 0.2811 and 0.1927 eV for the same sequence. The changes in TDM and ΔE of dimer CMC/ 2 OZn and dimer CMC/ 3 OZn model molecules are presented in table 2. Based on the obtained results, it can be concluded that the addition of ZnO with concentrations equal to or higher than those of CMC negatively affects the electronic properties of dimer CMC. As the changes that occurred in TDM and the ΔE are very small, in comparison with that of dimer CMC/ 1 OZn, we can conclude that the dimer CMC/ P2 OZn model molecule can be used in several applications due to the strong improvement in its electronic properties, and that the metal oxides should be added in small concentrations (not equal or larger than those of the polymer itself). This can be seen from the distribution of electrons within the dimer CMC/ P2 OZn model as the red colour intensity in the MESP maps increased as seen is figure 3-c and f in comparison with that in figure 10-c and d for dimer CMC/ 2 OZn and dimer CMC/ 3 OZn.

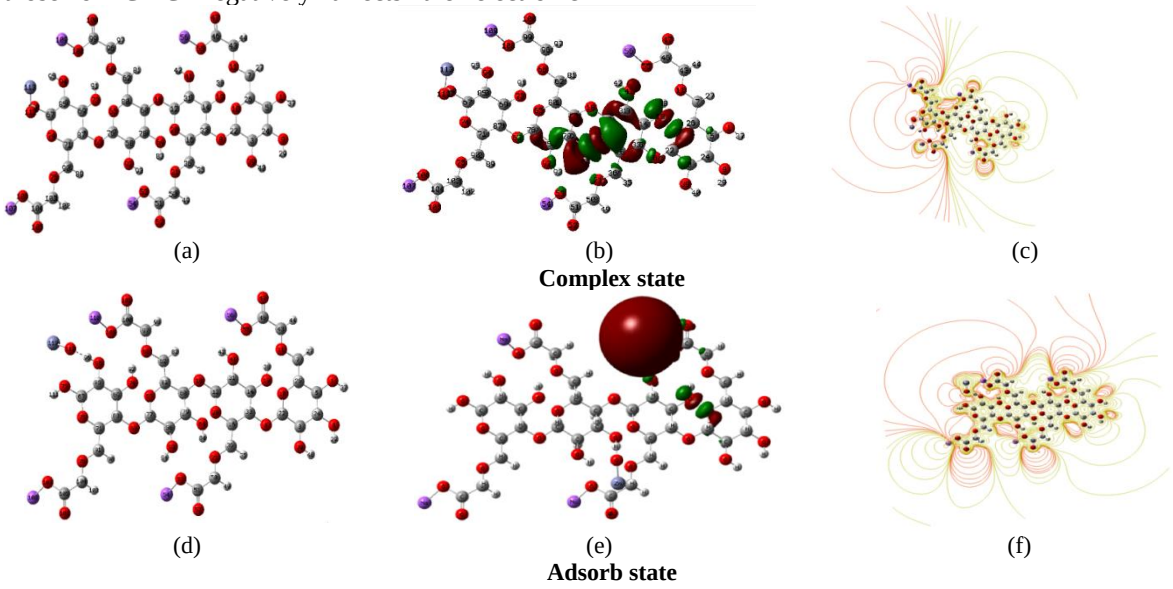

Fig.5.a) and d)- Optimized structure; b) and e)- HOMO-LUMO energy; and c) and f)- MESP maps calculated at B3LYP/LANL2DZ for dimer CMC/ P4 OZn in the two interaction mechanisms.

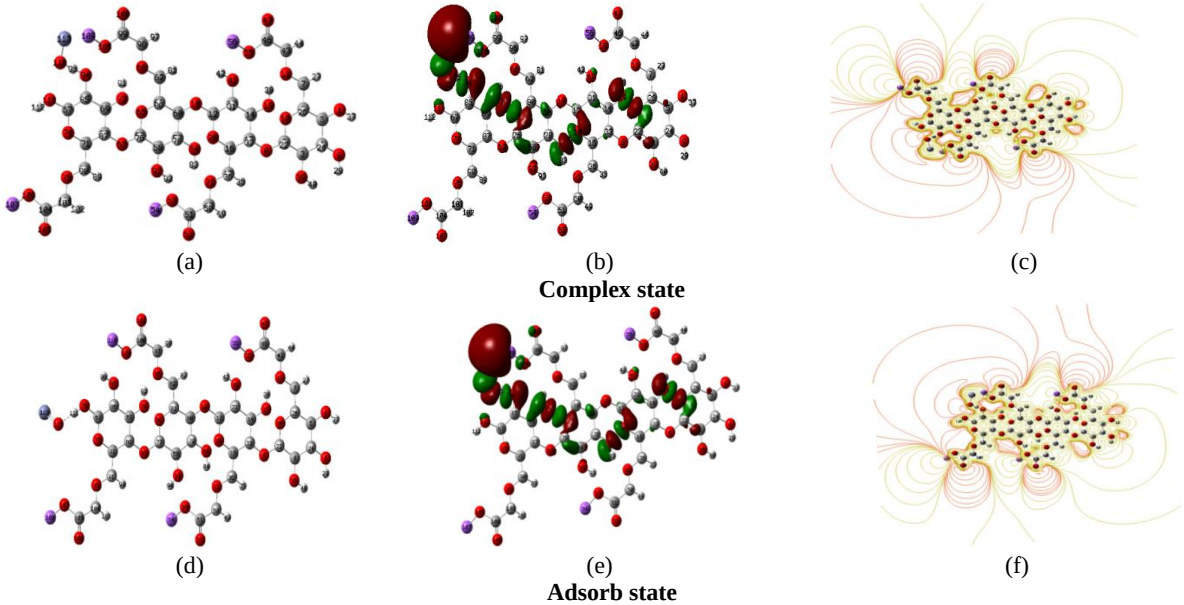

Fig. 6.a) and d)- Optimized structure; b) and e)- HOMO-LUMO energy; and c) and f)- MESP maps calculated at B3LYP/LANL2DZ for dimer CMC/ P5 OZn in the two interaction mechanisms.

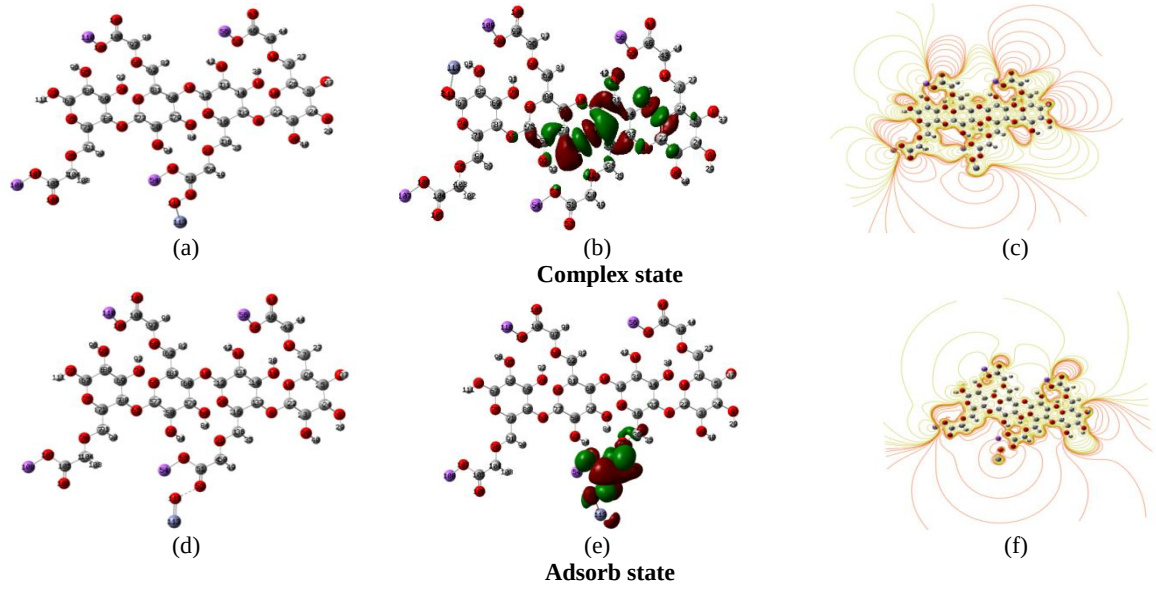

Fig. 7.a) and d)- Optimized structure; b) and e)- HOMO-LUMO energy; and c) and f)- MESP maps calculated at B3LYP/LANL2DZ for dimer CMC/ P6 OZn in the two interaction mechanisms.

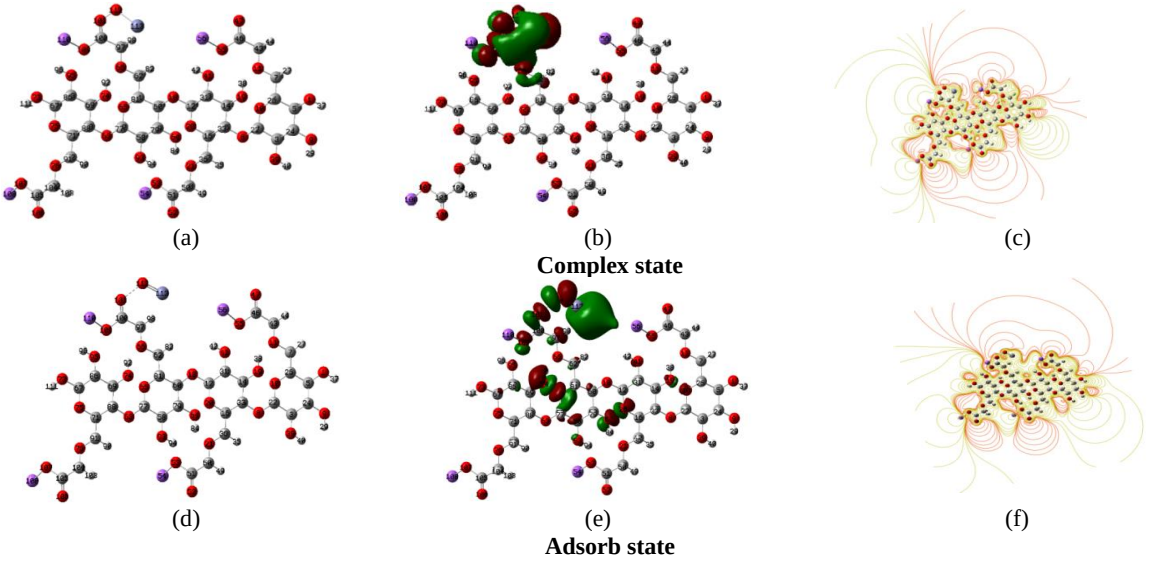

Fig. 8.a) and d)- Optimized structure; b) and e)- HOMO-LUMO energy; and c) and f)- MESP maps calculated at B3LYP/LANL2DZ for dimer CMC/ P7 OZn in the two interaction mechanisms.

1.3. Sensitivity of dimer CMC/1 OZn to NH_3gas

Due to the novel characteristics of ZnO, such as simple preparation, low cost, safety, and easy production andbased on the obtained results showing that the sensitivity of dimer CMCis improved by the addition of ZnO in comparison with that of dimer CMC;therefore, the model representingthe dimer CMC/1OZn can be used as a gas sensor. Accordingly, the sensitivity of dimer CMC/1OZn can be changed by the interaction with NH_3 gas. NH_3 is a natural gas, and it is a highly toxic chemical substance, that exists in the atmosphere in relatively low concentration. Recently, human activities have become the major source of NH_3 emissions. Motor vehicles and combustion of chemical plants are the main sources of NH_3 emissions. NH_3 sensors are used in medical diagnosis, chemical plants, food technology, and environmental protection. Accordingly, the design of sensors which allow fast and accurate detection of small concentrations of NH_3 gas is highly desirable [53].

NH_3 gas possesses TDM of 2.1335 Debye and ΔE of 9.1771 eV as presented in Table 3. Due to the exposure of dimer CMC/ OZn surface to NH_3 gas, changes take place in the dimer CMC/ 1 OZn electronic properties. The models representing NH_3 gas and CMC/ 1OZn/ 1 $NH_3$are presented in figure 11-a and b. Where, TDM increased by approximately twice its value and became28.7687 Debye while the ΔE decreased to0.2158 eV upon exposure to a single molecule of NH_3 gas. This is an indication of the sensitivity of the dimer CMC/ OZn surface to NH_3 gas. Therefore, it is concluded that dimer CMC/ OZn model molecule could be used as a sensor for NH_3 gas.

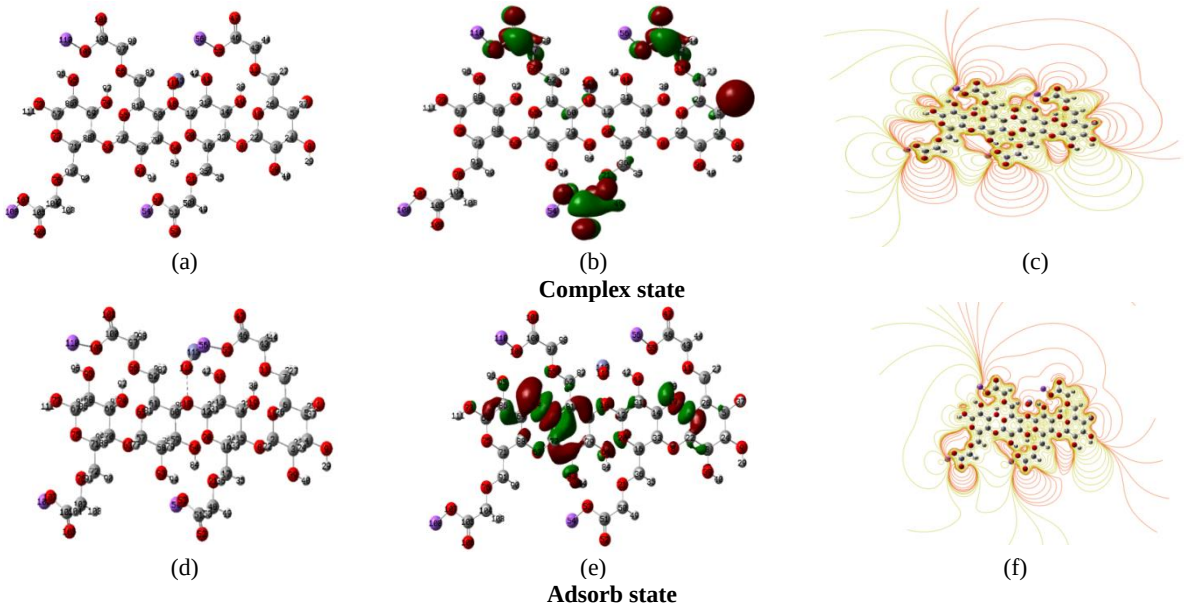

Fig. 9.a) and d)- Optimized structure; b) and e)- HOMO-LUMO energy; and c) and f)- MESP maps calculated at B3LYP/LANL2DZ for dimer CMC/ P8 OZn in the two interaction mechanisms.

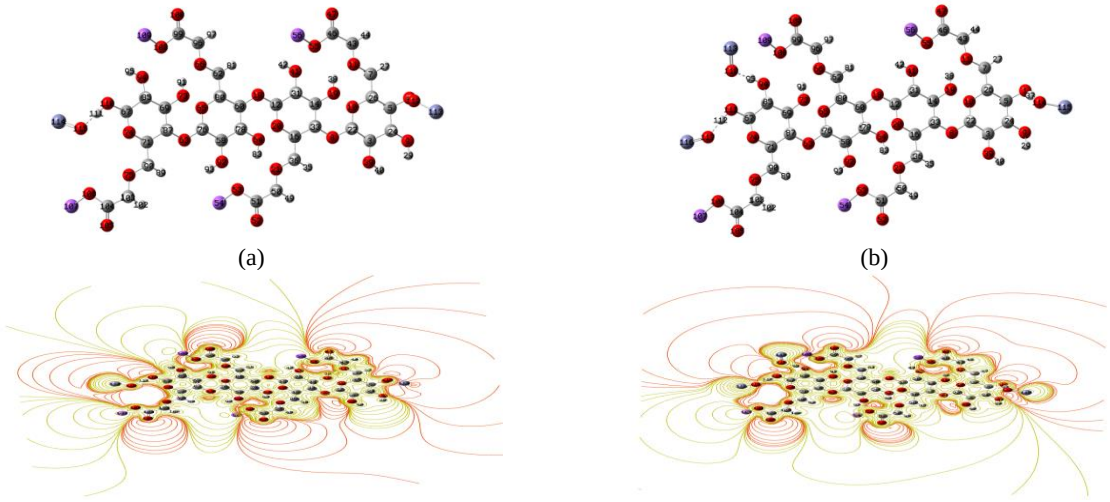

Fig. 10.Optimized structureof dimer CMC interacted with a)-2OZn and b)- 3 OZn and MESP maps calculated at B3LYP/LANL2DZ for CMC interacted with c)- 2 OZn and d)- 3 OZn.

1.4. Sensitivity of dimer CMC/1 OZn to H_2S gas

H_2S gas is a highly toxic, odorous, and strongly irritating gas. In the absence of serious sequelae, the maximum concentration of H_2S exposure, for one hour, is estimated to be between 170 and 300 ppm. The main sources of H_2S gas are decomposition of organic matter, volcanic gas, natural gas, petroleum, sewage treatment plants and sulfur deposits. Very little exposure to H_2S gas can cause nose/eye irritation and olfactory nerve paralysis. A moderate amount can cause a sore throat, cough, andchest tightness. Overexposure can cause disorientation, headaches, loss of reasoning, coma, seizures, and even death [55].

As presented in table 5, TDM and ΔE are calculated at the same level of theory. Figure 11- c and d shows the optimized structure of H_2S gas and dimer CMC/ 1OZn/ 1 H_2S. H_2S gas has TDM of 1.9390Debye and energy gap of 8.1940 eV. However, due to the interaction with dimer CMC, TDM reached to 31.5937 Debye. Meanwhile, ΔE changed to 0.2689 eV. The changes that occurred in the electronic properties of dimer CMC nanocomposites due to the exposure toH_2S gas confirm that CMC/ ZnO nanocomposites can be used as a sensor for H_2S gas.

1.5. Sensitivity of dimer CMC/1 OZn to HBr gas

Following the same scenario, the sensitivity of CMC/ZnO model molecule for HBr gas is also studied at the same level of theory. The hazards of

HBr gas lie in its high level of toxicity [55]. Based on the computations, it is found that HBr gas has TDM of 1.3416Debye and ΔEof 8.0748 eV as tabulated in table 6.TDM of dimer CMC/ P2 OZn changed to 32.8856 Debye while, the ΔEchanged to 0.2351 eV because of exposure to HBr gas. The optimized structure of HBr gas and CMC/ 1OZn/ 1 HBr are presented in figure 11-e and f.

Table 3 TDM as (Debye) and HOMO/LUMO energy gap as (eV) calculated at B3LYP/LANL2DZ for Dimer CMC and Dimer CMC/ X OZn throughout adsorb interaction where, X refers to the number of ZnO units interacted with dimer CMC, X= 2 and 3.

Structure	TDM (Debye)	ΔE (eV)
Dimer CMC/ 2OZn	12.7279	0.2811
Dimer CMC/ 3OZn	13.6132	0.1927

Table 4 TDM as (Debye) and HOMO/LUMO energy gap as (eV) calculated at B3LYP/LANL2DZ for NH3 gas, and CMC/ 1 OZn/ 1NH3.

Structure	TDM (Debye)	ΔE (eV)
NH_3	2.1335	9.1771
Dimer CMC/1OZn/ 1 NH_3	28.7687	0.2158

Table 5 TDM as (Debye) and HOMO/LUMO energy gap as (eV) calculated at B3LYP/LANL2DZ for H_2S gas, and CMC/ 1 OZn/ 1H_2S.

Structure	TDM (Debye)	ΔE (eV)
H_2S	1.9390	8.1940
Dimer CMC/1OZn/ 1 H_2S	31.5937	0.2689

Table 6 TDM as (Debye) and HOMO/LUMO energy gap as (eV) calculated at B3LYP/LANL2DZ for HBr gas, and CMC/ 1 OZn/ 1HBr.

Structure	TDM (Debye)	ΔE (eV)
HBr	1.3416	8.0748
Dimer CMC/1OZn/ 1 HBr	32.8856	0.2351

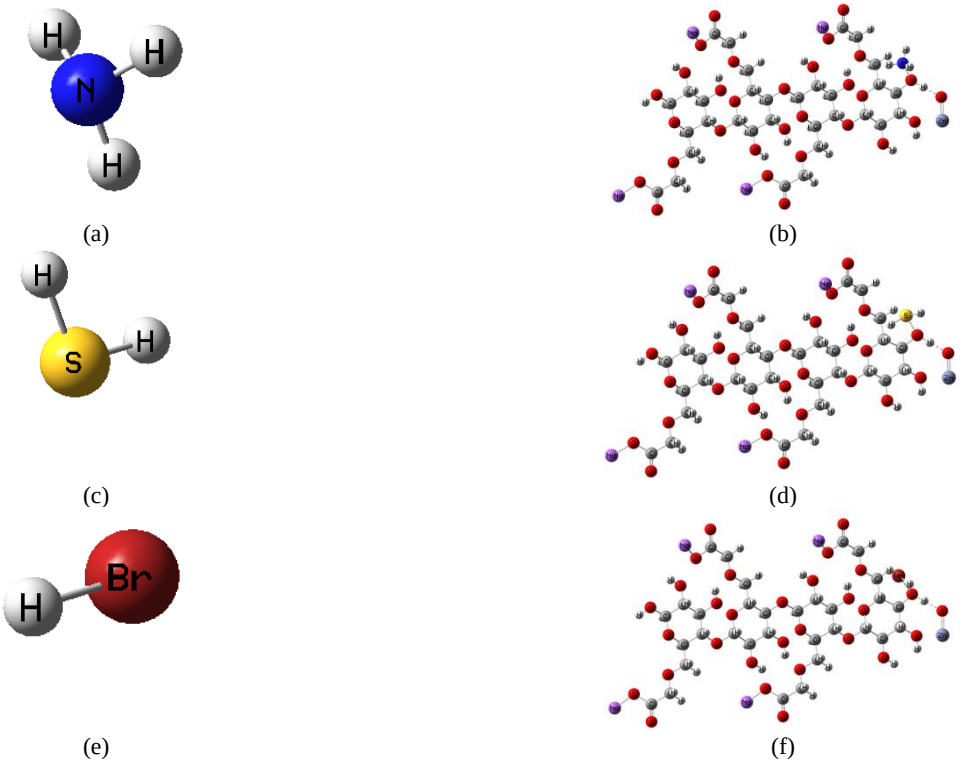

Fig. 11. The optimized structures of a)- NH_3 gas; b)- dimer CMC/ 1OZn/ 1 NH_3; c)- H_2S gas; d)- dimer CMC/ 1OZn/ 1 H_2S; e)- HBr gas; and f)- dimer CMC/ 1OZn/ 1 HBr.

Conclusions

The addition of nano metal oxides toa sensing material improves the gas-sensing properties of such material.In summary, we have studied and analyzed the interaction mechanism of ZnO on the surface of dimer CMC. DFT calculations were used to calculate the TDM, ΔEand MESP for the studied models.The results showed that the electronic properties of CMC are affected strongly upon the interaction with nanometal oxideas TDM increased to nearly 35 Debye. Also,after metal oxide complexation and adsorption, the dimer CMC ΔEis significantly reduced and reached half of its value (for dimer CMC/ P2 OZn model). Also, the results showed that the interaction can be adsorb more than complex.Furthermore, it is found that ZnO adsorption can improve the electronegativity of dimer CMCsurface.Considering the interaction with NH_3, H_2S and HBr gases, the adsorption of different gases

can effectively change the TDM and ΔEof dimer CMC/ OZn surface. According to thecharge distribution presented in the MESP maps, all studied gases transfer a large amount of charge to the atoms on the surface of dimer CMC/ OZn and then become negatively charged. Therefore, it could be concluded that CMC/ ZnO nanocomposite can be used as a sensor for NH_3, H_2S and HBr gases.

Conflicts of interest

The authors declare no conflict of interests, financial or otherwise.

References

[1] Taghizadeh S. M., Lal N., Ebrahiminezhad A., Moeini F., Seifan M., Ghasemi, Y. and Berenjian A., Green and economic fabrication of zinc oxide (ZnO) nanorods as a broadband UV blocker and antimicrobial agent. *Nanomaterials*, 10(3), 530 (2020).

[2] Politi J. R. S., Martins J. B. L. and Cabral, B. J. C., A first principles approach to the interactions of alkali metal atoms with carbon quantum dots. *Computational Materials Science*, **197**, 110614 (2021).

[3] Diao Y., Liu L., Xia S., Feng S. and Lu F., Study on electronic and optical properties of alkali metal atoms adsorbed GaAs nanowires by first-principles calculations. *Solid State Communications*, **278**, 42-48 (2018).

[4] Das S. and Srivastava V. C., An overview of the synthesis of CuO-ZnO nanocomposite for environmental and other applications. *Nanotechnology Reviews*, **7**(3), 267-282 (2018).

[5] Yu X., Marks T. J. and Facchetti A., Metal oxides for optoelectronic applications. *Nature materials*, **15**(4), 383-396 (2016).

[6] Kumar R., Al-Dossary O., Kumar G. and Umar A., Zinc oxide nanostructures for NO 2 gas–sensor applications: A review. *Nano-Micro Letters*, **7**(2), 97-120 (2015).

[7] Leonardi S. G., Two-dimensional zinc oxide nanostructures for gas sensor applications. *Chemosensors*, **5**(2), 17 (2017).

[8] Chiu Y. H., Chang K. D. and Hsu Y. J., Plasmon-mediated charge dynamics and photoactivity enhancement for Au-decorated ZnO nanocrystals. *Journal of Materials Chemistry A*, **6**(10), 4286-4296 (2018).

[9] Huy N. N., Thuy V. T. T., Thang N. H., Thuy N. T., Khoi T. T. and Van Thanh D., Facile one-step synthesis of zinc oxide nanoparticles by ultrasonic-assisted precipitation method and its application for H2S adsorption in air. *Journal of Physics and Chemistry of Solids*, **132**, 99-103 (2019).

[10] Carp O., Tirsoaga A., Ene R., Ianculescu A., Negrea R. F., Chesler P. and Birjega R., Facile, high yield ultrasound mediated protocol for ZnO hierarchical structures synthesis: formation mechanism, optical and photocatalytic properties. *Ultrasonics sonochemistry*, **36**, 326-335 (2017).

[11] Sornalatha D. J., Bhuvaneswari S., Murugesan S. and Murugakoothan P., Solochemical synthesis and characterization of ZnO nanostructures with different morphologies and their antibacterial activity. *Optik*, **126**(1), 63-67 (2015).

[12] Abdel-Gawad F. K., Osman O., Bassem S. M., Nassar H. F., Temraz T. A., Elhaes H. and Ibrahim M., Spectroscopic analyses, and genotoxicity of dioxins in the aquatic environment of Alexandria. *Marine pollution bulletin*, **127**, 618-625 (2018).

[13] Kaur R., Singh A. V., Sehrawat K., Mehra N. C. and Mehra, R. M., Sol–gel derived yttrium doped ZnO nanostructures. *Journal of non-crystalline solids*, **352**(23-25), 2565-2568 (2006).

[14] Kubota J., Haga K., Kashiwaba Y., Watanabe H., Zhang B. P. and Segawa Y., Characteristics of ZnO whiskers prepared from organic-zinc. *Applied surface science*, **216**(1-4), 431-435 (2003).

[15] Wang Z. L., Nanostructures of zinc oxide. *Materials today*, **7**(6), 26-33 (2004).

[16] Dhanalakshmi A., Natarajan B., Ramadas V., Palanimurugan A. and Thanikaikarasan S., Structural, morphological, optical and antibacterial activity of rod-shaped zinc oxide and manganese-doped zinc oxide nanoparticles. *Pramana*, **87**(4), 1-9 (2016).

[17] Wu C., Qiao X., Chen J., Wang H., Tan F. and Li, S., A novel chemical route to prepare ZnO nanoparticles. *Materials Letters*, **60**(15), 1828-1832 (2006).

[18] Alghunaim N. S., Omar A., Elhaes, H. and Ibrahim M., Effect of ZnO and TiO2 on the reactivity of some polymers. *Journal of Computational and Theoretical Nanoscience*, **14**(6), 2838-2843 (2017).

[19] Ibrahim M. and Elhaes H., Computational spectroscopic study of copper, cadmium, lead and zinc interactions in the environment. *International journal of environment and pollution*, **23**(4), 417-424 (2005).

[20] Ibrahim M., Modeling the Effect of Zinc Oxide on the Electronic Properties of Polyvinyl Alcohol. *Egyptian Journal of Chemistry*, **63**(12), 3-5 (2020).

[21] Abd Elhady M. M., Preparation, and characterization of chitosan/zinc oxide nanoparticles for imparting antimicrobial and UV protection to cotton fabric. International journal of carbohydrate chemistry, 2012 (2012).

[22] Badry R., Fahmy A., Ibrahim A., Elhaes H. and Ibrahim M., Application of polyvinyl alcohol/polypropylene/zinc oxide nanocomposites as sensor: modeling approach. *Optical and Quantum Electronics*, **53**(1), 1-12 (2021).

[23] Kadir M. F. Z., Majid S. R. and Arof, A. K., Plasticized chitosan–PVA blend polymer electrolyte based proton battery. *Electrochimica Acta*, **55**(4), 1475-1482 (2010).

[24] Samsudin A. S., Khairul W. M. and Isa M. I. N., Characterization on the potential of carboxy methylcellulose for application as proton conducting biopolymer electrolytes. *Journal of Non-crystalline solids*, **358**(8), 1104-1112 (2012).

[25] Badry R., Ezzat H. A., El-Khodary S., Morsy M., Elhaes H., Nada N. and Ibrahim M. Spectroscopic and

thermal analyses for the effect of acetic acid on the plasticized sodium carboxymethyl cellulose. *Journal of Molecular Structure*, **1224**, 129013 (2021).

[26] Badry R., El-Khodary S., Elhaes H., Nada N. and Ibrahim M., Optical, conductivity and dielectric properties of plasticized solid polymer electrolytes based on blends of sodium carboxymethyl cellulose and polyethylene oxide. *Optical and Quantum Electronics*, **53**(1), 1-15 (2021).

[27] Kulikowska A., Wasiak I. and Ciach T., Synthesis of carboxymethylcellulose nanoparticles using various coiling agents. Prosimycytowaćjako: Inz. *Ap. Chem*, **53**(4), 268-269 (2014).

[28] Ahmad, N. H., & Isa, M. I. N., Ionic conductivity, and electrical properties of carboxymethyl cellulose-NH4Cl solid polymer electrolytes. *Journal of Engineering Science and Technology*, **11**(6), 839-847 (2016).

[29] Zainuddin N. K. and Samsudin A. S.,Electrical properties studies of solid polymer electrolytes membrane based on carboxymethyl cellulose (CMC)/kappa carrageenan blend. *In AIP Conference Proceedings (AIP Publishing LLC)*, 2030(1) 020222 (2018).

[30] Ali G. W., Abdel-Fattah W. I., Elhaes H. and Ibrahim M. A., Spectroscopic and modeling analyses of bimolecular structure of corn silk. *Biointerface Research of Applied Chemistry*, **9**, 4581-4585 (2019).

[31] Ezzat H. A., Elhaes H. Refaat A. Abdel-Aal M. S. and Ibrahim M. A., Molecular Modeling Analyses and Vibrational Characteristics for Nitromethane. *Egyptian Journal of Chemistry*, **64**(1), 75-84 (2021).

[32] Badry R., Radwan S. H., Ezzat D., Ezzat H., ElhaesH. and Ibrahim M. Study of the Electronic Properties of Graphene Oxide/(PANi/Teflon). *Biointerface Research in Applied Chemistry*, **10**, 6926-6935 (2020).

[33] Ezzat H. A., Hegazy M. A., Nada N. A., Osman O. and Ibrahim M. A., Application of natural polymers enhanced with ZnO and CuO as humidity sensor. *NRIAG Journal of Astronomy and Geophysics*, **9**(1), 586-597 (2020).

[34] Bayoumy A. M., Elhaes H., Osman O., Ibrahim M. A., Kholmurodov K. T. and Hussein T. Effect of nano metal oxides on heme molecule: molecular and biomolecular approaches. *BiointerfaceResearch in Applied Chemistry*, **10**(1), 4837-4845 (2019).

[35] Ibrahim A., Elhaes H., Ibrahim M., Yahia I. S. and Zahran H. Y., Molecular modeling analyses for polyvinylidene X (X= F, Cl, Br and I). *BiointerfaceResearch in Applied Chemistry*, **9**, 3890-3893 (2019)

[36] Badry R., Shaban H., Elhaes H., Refaat A. and Ibrahim M. Molecular modeling analyses of polyaniline substituted with alkali and alkaline earth elements. *Biointerface Research in Applied Chemistry*, **8**(6), 3719-3724 (2018).

[37] Ibrahim M., Osman O. and Mahmoud A. A., Spectroscopic analyses of cellulose and chitosan: FTIR and modeling approach. *Journal of Computational and Theoretical Nanoscience*, **8**(1), 117-123 (2011).

[38] Ibrahim M. A., Elhaes H., El-Khodary S. A., Morsy M., Refaat A., Yahia I. S. and Zahran H. Y., Molecular modeling analyses for the effect of alkali metal oxides on graphene. *Biointerface Research in Applied Chemistry*, **8**(5), 3522-3525 (2018).

[39] Becke A.D., Density-functional thermochemistry. III. The role of exact exchange, *Journal of Chemical Physics*, **98**, 5648–5652 (1993).

[40] Becke A.D., Density-functional thermochemistry IV. A new dynamical correlation functional and implications for exact-exchange mixing. *Journal of Chemical Physics*, **104**, 1040–1046 (1996).

[41] Lee C., Yang W., Parr R.G., Development of the Colle-Salvetti correlation-energy formula into a functional of the electron density. *Physical Review B*,**37**, 785–789 (1988).

[42] Foresman J. and Frish E., *Exploring chemistry. Gaussian Inc.* Pittsburg, USA (1996).

[43] Vosko S. H., Wilk L. and Nusair M., Accurate spin-dependent electron liquid correlation energies for local spin density calculations: a critical analysis. *Canadian Journal of physics*, **58**(8), 1200-1211 (1980).

[44] Frisch M.J., Trucks G.W., Schlegel H.B., Scuseri G.E, Robb M.A., Cheeseman J.R., Scalmani G., Barone V., Mennucci, Petersson B. G. A., Nakatsuji H., Caricato M., Li X., HratchianP.H., Izmaylov A.F., Bloino J., Zheng G., Sonnenberg J.L., Hada M.,Ehara M., Toyota K., Fukuda R., Hasegawa J., Ishida M., Nakajima,T . Honda Y., Kitao O., Nakai H., Vreven T., Montgomery J.A., Jr., Peralta J.E., Ogliaro F., Bearpark M., Heyd J.J., Brothers, E. Kudin K.N., Staroverov V.N., Keith T., Kobayashi R., Normand,J. , Raghavachari K.,, Rendell A.,, Burant J.C., Iyengar S.S., Tomasi J.,, Cossi M., Rega N., Millam J.M., Klene M., Knox J.E., Cross J.B.,, Bakken V., Adamo C., Jaramillo J., Gomperts R., Stratmann R.E.,, Yazyev O., Austin A.J., Cammi R., Pomelli C., Ochterski J.W., , Martin R.L., Morokuma K., Zakrzewski V.G., Voth G.A., Salvador P., Dannenberg J.J., Dapprich S., Daniels A.D., , Farkas, O., Foresman J.B., Ortiz J.V., Cioslowski J.,, Fox D.J., Gaussian, Inc., Gaussian 09, Revision C.01.Wallingford CT (2010).

[45] Badry R., Ibrahim A., Gamal F., Shehata D., Ezzat H., Elhaes H. and Ibrahim M., Electronic Properties of Polyvinyl Alcohol/TiO2/SiO2Nanocomposites.*Biointerface Research in. Applied. Chemistry*, **10**, 6427-6435 (2020).

[46] Fahmy A., Khafagy R. M., Elhaes H.andIbrahim M. A**.,** ICMMS-2: Molecular Modeling Analyses of Polyvinyl Alcohol/Sodium Alginate/ZnO Composite. *Egyptian Journal of Chemistry*, 64(3), 7-8(2021).

[47] Moez A. A., Fahmy A., Ezzat H., Ibrahim A. M., Shehata D., Elhaes H.andIbrahim M. A., Molecular Modeling Analyses for Polypropylene/Zinc Oxide Nanocomposite. *Biointerface Research in Applied Chemistry*, **11**(4), 11347 - 11356 (2020).

[48] Ezzat H. A., Hegazy M. A., Nada N. A., Osman O.andIbrahimM. A**.,** ICMMS-2: Application of Cs/ZnO/GO Hybrid Nanocomposite for Enhanced Inter-behavior of Electronic Properties and Thermal Stability as Corrosion Inhibitor. *Egyptian Journal of Chemistry*, 64(3), 1197-1205(2021).

[49] Politzer P., Laurence P. R**.** and Jayasuriya K**.,** Molecular electrostatic potentials: an effective tool for the elucidation of biochemical phenomena. *Environmental health perspectives*, 61, 191-202(1985).

[50] Pullman A.andPullman B**.,** Molecular electrostatic potential of the nucleic acids. *Quarterly reviews of biophysics*, 14(3), 289-380(1981).

[51] Weiner PK, Langridge R, Blaney JM, Schaefer R, Kollman PA., Electrostatic potential molecular surfaces. *Proceedings of the National Academy of Sciences*,**79**(12):3754–3758 (1982).

[52] Bielecki Z., Stacewicz T., Smulko J. and Wojtas J., Ammonia Gas Sensors: Comparison of Solid-State and Optical Methods. *Applied Sciences*, **10**(15), 5111 (2020).

[53] Bari R. H., Patil P. P., Patil S. B. and Bari A. R., Detection of H 2 S gas at lower operating temperature using sprayed nanostructured In 2 O 3 thin films. *Bulletin of Materials Science*, **36**(6), 967-972 (2013).

[54] Khan M. A. H., Rao M. V. and Li Q., Recent advances in electrochemical sensors for detecting toxic gases: NO2, SO2 and H2S. *Sensors*, **19**(4), 905 (2019).

[55] Lee B. J., Efremov A. and Kwon K. H., Plasma parameters, gas-phase chemistry and Si/SiO2 etching mechanisms in HBr+ Cl2+ O2 gas mixture: Effect of HBr/O2 mixing ratio. *Vacuum*, **163**, 110-118 (2019).